Journal of Materials Chemistry C

ROYAL SOCIETY OF CHEMISTRY

PAPER

View Article Online
View Journal | View Issue

Cite this: J. Mater. Chem. C, 2025, 13, 22702

Iron tetraphenylporphyrin chloride–metal substrate interaction mediated by a graphene buffer layer

Abhishek Kumar,†[ab] Matus Stredansky,‡[a] M. Panighel,§[a] Federica Bondino,[a] Elena Magnano,[a] Silvia Nappini,[a] Igor Píš,[ac] L. Cozzarini,¶[a] A. Nefedov,[d] Andrea Goldoni,[c] C. Cepek[a] and M. Pedio*[a]

We investigate the interfacial electronic structure of monolayer iron tetraphenylporphyrin chloride (FeTPP–Cl) adsorbed on graphene (Gr) buffer layers supported by Ni(111) and Pt(111). This study unveils the role of a graphene buffer layer in controlling the charge transfer mechanisms of self-assembled porphyrins on metal surfaces, reshaping interfacial energy level alignment, charge transfer dynamics, interface dipoles, and charge injection barriers. By exploiting the intrinsic n- and p-type doping of graphene on Ni and Pt, we modulate the charge transfer behavior in iron tetraphenylporphyrin monolayers, using these systems as model platforms to probe interfacial electronic processes and the impact of graphene–substrate coupling. Through a comprehensive multi-technique approach, combining X-ray photoemission, ultraviolet photoemission, and X-ray absorption spectroscopies, we demonstrate how substrate-induced doping drives significant changes at the molecule–graphene–metal interface. Core-level binding energies (BEs) and ionization potentials (IPs) indicate weak physisorption in both systems, with opposite charge transfer directions depending on the substrate, despite similar molecular morphologies. On Gr/Ni(111), all core levels shift to higher BE, with a pronounced +0.6 eV shift in Fe 2p and a +0.15 eV IP increase, indicating electron transfer from the substrate to the molecule localized at the Fe center. On Gr/Pt(111), C 1s and N 1s shift to lower BE and the IP decreases by −0.15 eV, consistent with electron donation from the molecule to the substrate, more delocalized on the macrocycle. The small interface dipoles (−0.15 eV for Ni, −0.25 eV for Pt) and the absence of rigid shifts demonstrate that charge redistribution is fractional and site-specific, governed primarily by electrostatics and graphene doping rather than strong hybridization. These findings suggest that the interaction strength and electronic behavior at the interface are governed by the underlying metal, with Gr acting as an effective electronic decoupler or mediator. Our study highlights the importance of the graphene–metal interface in modulating charge transfer and level alignment in porphyrin-based hybrid systems.

Received 19th May 2025,
Accepted 7th October 2025

DOI: 10.1039/d5tc01982f

rsc.li/materials-c

Introduction

Organic electronics have gained increasing attention in the surface science community in recent decades, driven by the promise of lightweight, cost-effective, and flexible electronic devices. The maturity of the organic light-emitting diode OLED technology that has already reached the market has further increased the expectations in organic electronics, underscoring the importance of understanding and engineering the interfaces between organic materials and inorganic (often metallic) substrates.[1] Indeed, at the interface, charges are exchanged (injected or extracted), dictating the electronic properties of the whole device. In this perspective, great effort has been made to characterize and modify the electronic structure of the interface. The interface morphology is crucial for charge injection

[a] CNR - Istituto di officina dei materiali (IOM), Consiglio Nazionale delle Ricerche, Trieste, 34149, Italy. E-mail: pedio@iom.cnr.it
[b] Department of Physics, University of Trieste, Italy
[c] Elettra Sincrotrone Trieste, Area Science Park Basovizza, Trieste, 34149, Italy
[d] Institute of Functional Interfaces, Karlsruhe Institute of Technology, Eggenstein-Leopoldshafen, 76344, Germany
† Present address: Department of Physics, Chandigarh University, Chandigarh, India.
‡ Present address: Department of Chemistry, University of Birmingham, Birmingham, England, GB.
§ Present address: Scanning Probe Microscopy Laboratory, Department of Physics and Materials Science, University of Luxembourg, Luxembourg City L-1511, Luxembourg.
¶ Present address: Dipartimento di Ingegneria e Architettura, Università degli Studi di Trieste, 34127 Trieste, Italy.

and extraction, directly impacting device performance. In some cases, amorphous layers are preferable (OLEDs),[2] whereas highly ordered phases are beneficial for application in organic photovoltaics[3] or organic field-effect transistors.[4] In this context, graphene (Gr) has been proven to act as a template for organic molecules, inducing flat adsorption geometry due to the high face-to-face interaction with aromatic molecules. The use of Gr as a buffer layer on metal surfaces provides access to its outstanding mechanical and electronic properties[5] like high tensile strength and Young's modulus ($\sim$1 TPa),[6] and high electron mobility (200 000 $cm^2\ V^{-1}\ s^{-1}$),[7] together with high thermal conductivity (up to 5300 $W\ m^{-1}\ K^{-1}$)[8] and surface area.[9]

The electronic structure of the supported graphene is profoundly influenced by its underlying metal substrate,[10] which affects the degree of hybridization, doping, and π–electron coupling.[11–13] Unlike free-standing Gr, metal-supported graphene can exhibit either n-type or p-type doping as a result of charge transfer. For instance, Gr on nickel (Ni), a relatively strong chemisorptive bond is formed, and typically Gr displays an n-type doping due to electron donation from the Ni d-states into the Gr π-structure, leading to a high degree of hybridization.[14,15] In contrast, Gr on platinum (Pt), where the interaction is weaker and more physisorptive, is weakly p-doped due to minor hole transfer from the substrate.[16,17] Structural differences also arise, with Gr/Pt(111) displaying a Moiré pattern and a layer distance of 0.31 nm, compared with the 0.21 nm spacing of Gr/Ni(111). These differences in doping significantly alter the electronic properties at the interface, making Gr an ideal platform for assembling organic molecules like planar porphyrins, and π-conjugated macrocycles with rich optical and electronic characteristics.[18] The Gr buffer layer serves as an atomically flat and chemically inactive surface for controlled porphyrin assembly *via* non-covalent interactions.[19] The nature of the Gr–metal interaction is decisive in determining the strength of molecule–substrate coupling, the extent of charge transfer, and the resulting electronic structure of the hybrid system.

It is worth noting that in the case of molecular adsorption on metal surfaces, the molecule–substrate interactions can prevail over the intermolecular ones, thereby preventing the formation of self-assembled structures, as in the case of iron tetraphenyl porphyrin chloride (FeTPP–Cl, $C_{44}H_{28}N_4FeCl$) on Ni(111).[20] In this regard, the Gr buffer layer facilitates the self-assembly process, providing a pathway to engineer molecular electronic properties.

Tetrapyrroles and their derivatives represent a widely investigated class of molecules for their well-defined shape, thermal stability and seemingly limitless potential for chemical functionalization.[18] Due to their versatility, they have been proposed for applications in heterogeneous (photo)catalysis[21–23] electrocatalysis,[24] sensors[25] and organic electronics.[26] Iron(III) tetraphenylporphyrin and its derivatives are extensively studied for their role in the electrochemical CO_2 reduction reaction. Modifications to the FeTPP structure and its immobilization on graphene, carbon black or other novel materials have been investigated to enhance its efficiency and selectivity in producing CO.[27] Moreover, FeTPP-based catalysts exhibit promising activity for the oxygen reduction reaction.[28]

Understanding how Gr doping influences molecular electronic states is crucial for device optimization. The use of a graphene buffer layer between phthalocyanine or porphyrin and a metal substrate has been studied for various systems.[29,30] In particular, comparative studies of cobalt phthalocyanine (CoPc) on Gr/Ni(111) and Gr/Pt(111)[31] revealed that the graphene buffer layer reduces the interaction between CoPc and Pt(111), while for Gr/Ni(111), a strong charge transfer takes place. This charge transfer was only suppressed by intercalating gold, which reduces electron donation from Ni(111) into graphene. These results demonstrate that charge transfer strongly depends on the underlying metal substrate. Single layers of FePc on Gr/Ni(111) studies[32,33] show that the charge transfer (electrons from Gr/Ni to an Fe-related unoccupied orbital of FePc) is not completely suppressed by the introduction of a graphene buffer layer between phthalocyanine and Ni(111). However, a non-covalent interaction with the substrate takes place.

The present study focuses on the interaction between FeTPP–Cl and the Gr buffer layer. The presence of the four peripheral phenyl rings could act as a spacer, likely resulting in a different situation from the FePc case.

This paper investigates the structural and electronic properties of the Gr buffer layer on metal supports, focusing on its role in tuning interfacial charge transport, which is essential for hybrid graphene-organic systems. Here, we explore these effects by studying FeTPP–Cl on two distinct graphene–metal interfaces: Gr/Ni(111) and Gr/Pt(111), focusing on the role of the graphene buffer layer in tuning interfacial charge transport.

A change in the molecular packing could influence the energy levels of the film, the ionization potential and the interface dipole (see, for example, ref. 34). For this reason, we investigated the single-layer FeTPP–Cl systems, which we found to have the same morphology when deposited onto both Gr/Ni and Gr/Pt substrates.

Theoretical studies have previously examined FeTPP or related metalloporphyrins on graphene substrates. Song *et al.*[35] reported weak physisorption and minimal charge transfer ($\sim$0.04 e) for FeTPP–Cl on pristine Gr, indicating electronic decoupling and preservation of the molecule's character. Touzeau *et al.*[36] found that even within weakly interacting systems, charge redistribution can occur depending on metal centers or functional groups. These studies provide a useful foundation for understanding how FeTPP–Cl may interact with graphene-based supports in more complex environments.

Our goal is to harness the unique properties of graphene to modulate the interfacial electronic behavior and exert control over charge transfer, injection barriers, and charge transport, which are crucial parameters for the advancement of next-generation organic electronic devices.

Results

Morphology and molecular assembly

The systems were grown in UHV and characterized as described in section S1 of the SI. The quality of the graphene layers was monitored using photoemission, near-edge X-ray absorption

fine structure (NEXAFS) C K edge, and LEED. See paragraph S2 for details. We emphasize that FeTPP–Cl exhibits a layer-by-layer growth mode on both Gr/Ni(111) and Gr/Pt(111) substrates, and for a 1 monolayer (ML) coverage, a hexagonal LEED pattern was detected in both cases.

NEXAFS measurements were conducted at the N and C K edges of bare Gr/Me and for FeTPP–Cl/Gr/Ni(111) and FeTPP–Cl/Gr/Pt(111) and the multilayer. The spectra collected at different incidence angles provide insights into the orbital dichroism, yielding an evaluation of the molecular average tilt angle.

N K edge NEXAFS spectra at different geometries are shown in Fig. S3 for both metal substrates. The tilt angle has been evaluated following a standard procedure[37] and considering the polarization of the impinging light. By fitting the LUMO dichroism as a function of the linear polarization angle, the average tilt angle of the macrocycle is obtained. Slight differences are observed in FeTPP–Cl on Gr/Ni(111) and Gr/Pt(111), with tilt angles of $5^\circ \pm 5^\circ$ and $0^\circ \pm 5^\circ$, respectively, between the molecular macrocycle and the substrate. It is worth noting that no variation in the lineshape of the LUMO for the 1 ML systems has been revealed in comparison with the multilayer spectra (Fig. S4).

The π*-region of NEXAFS spectra measured at C K edges (Fig. 1) of the molecular layers in both cases were obtained after subtracting the C K-edge contribution of the respective graphene substrates (see paragraph S2 in the SI).

The C K-edge for FeTPP–Cl adsorbed on Gr/Ni(111) shows a first peak at 284.6 eV. According to the literature, this peak is related to a transition from the core of the C atoms in the macrocycle to the π* orbitals.[38,39] The second double peak at about 285.4 eV is assigned to the transition from the C 1s orbital of carbon to the empty π* orbitals of the phenyl rings. In the case of Gr/Pt(111) the C K edge shows a line shape almost similar to that of Gr/Ni(111). The macrocycle, in both samples, shows a strong dichroism, in agreement with N K-edge analysis, confirming its adsorption parallel to the graphene layer.

By contrast, we found an opposite dichroism of the phenyl features in the C K-edge spectra, in comparison with the macrocycle. Such a finding indicates that phenyl groups are tilted with respect to the substrate.

The analysis of the phenyl dichroism performed following the procedure used in ref. 38 and 39 found an average angle of $65^\circ \pm 5^\circ$ for both 1 ML FeTPP–Cl on the Ni and Pt systems, confirming the similarities between the two systems. This observation found agreement with theoretical calculations for the tetraphenyl porphyrin layers on graphene.[40]

FeTPP–Cl is known to undergo Cl atom loss (dechlorination) when adsorbing on metal substrates.[41] The molecule dechlorination is incomplete for deposition at room temperature (RT) on both the Gr/Me (Me = Ni, Pt) substrates, up to 1 ML, with a fraction of about 25% of the molecules still presenting a Cl signal similar for both the Gr/Me substrates. Thermal treatment in UHV at 270 °C–280 °C completely removes the Cl atom, although it introduces variations in the photoemission BE data compared with the as-deposited spectra. We focus here on the role of the Gr buffer layer, and we do not discuss the annealed interfaces in the present analysis. The kinetics of dechlorination and the annealing effects on the FeTPP/Gr interfaces will be discussed in a forthcoming paper.

Valence band and vacuum level alignment: photoemission measurements

Valence band and energy level alignments were characterized using photoemission and secondary electron cutoff measurements.

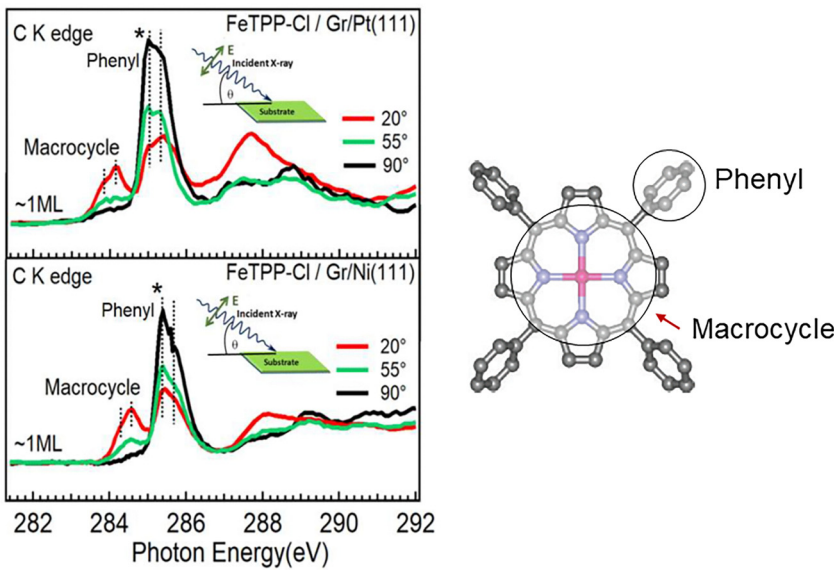

Fig. 1 Left: C K-edge of 1 ML FeTPP–Cl/Gr/Pt(111), upper panel, and FeTPP–Cl/Gr/Ni(111), lower panel. The spectra have been obtained after subtraction of the bare graphene measurements. At normal incidence (90°), the data were acquired with the incoming photons perpendicular to the sample surface, resulting in the polarization vector lying parallel to the surface plane. At grazing incidence (20°), the photons arrive at the surface at a shallow angle, with the polarization vector oriented nearly perpendicular to the surface plane. Right: structure of the tetraphenyl porphyrin, the circles indicate the central macrocycle and the external phenyl groups.

Valence band (VB) spectra of 1 ML FeTPP–Cl/Gr/Ni(111) and FeTPP–Cl/Gr/Pt(111), acquired with He II (40.8 eV)[42] and 46 eV[43] photons, are presented in Fig. 2a alongside reference spectra of bare graphene on both substrates and the FeTPP–Cl multilayer. On both substrates, characteristic graphene features are observed, with the π band located at approximately 10 eV from the Fermi level for Ni (n-doped graphene ref. 14 and 15) and 8 eV for Pt (p-doped graphene ref. 16 and 17).

In the FeTPP–Cl free molecule, Cl exhibits an oxidation state of −1, while Fe is in the +3 oxidation state. In the multilayer regime, the highest occupied molecular orbital (HOMO) and HOMO−1 are attributed to the tetrapyrrole ring (R) and phenyl groups (Ph), respectively.[39,44] Their binding energies (BE) align with those of FeTPP (chlorine-free), typically observed only after metalation of the metal-free tetraphenyl porphyrin.[18,45,46] Compared to metal-free H_2TPP films,[47] FeTPP–Cl exhibits more complex features at high BE. Photon energy-dependent spectra (Fig. S6) reveal additional peaks at high BE, attributed to photoemission cross-section effects. Theoretical calculations48 indicate that the Fe center contributes to the electronic states across a broad energy range (0–10 eV BE), while Cl contributes primarily to the HOMO−2 at ∼5 eV BE.[49]

At 1 ML coverage, the molecular features remain largely intact. However, non-rigid shifts are detected: the HOMO–HOMO−1 energy separation increases on Ni and decreases on Pt by ∼0.2 eV (Fig. 2c), suggesting a substrate-dependent redistribution of charge within the molecule.

To further probe the substrate–molecule interaction, we measured the hole injection barriers and work functions (WF) of the clean graphene substrates, 1 ML films, and multilayer, using secondary electron cutoff spectroscopy (Fig. S5). For the bare substrates, the work functions are 4.6 eV for Gr/Pt(111) and 4.2 eV for Gr/Ni(111), consistent with the literature values.[50] The WF of the multilayer is 4.25 eV. Upon FeTPP–Cl deposition, interface dipoles (ΔWF) arise from changes in WF. The hole injection barrier (Δh) is defined as the energy difference between the Fermi level and the HOMO onset. Table 1 summarizes the HOMO, HOMO−1, WF, ionization potential (IP *i.e.*, the sum of the monolayer work function WF and the molecular HOMO binding energy onset), and Δh for all systems.

The measured ionization potentials for FeTPP adsorbed on graphene/metal substrates reveal substrate-dependent electronic interactions. Compared to the multilayer reference (5.1 eV), FeTPP on Gr/Ni exhibits an increased IP (5.25 eV), while FeTPP on Gr/Pt shows a reduced IP (4.95 eV).

In the case of 1 ML FeTPP–Cl/Gr/Ni(111), a redistribution of charge in the molecular conjugated system takes place with the appearance of an interface state Is close to the Fermi level. This state is distinguishable for 0.5 ML and 1 ML, as shown in Fig. 3, but disappears for higher coverages. Similar interface states have been previously reported for iron phthalocyanine (FePc) on Gr on Ni,[51] FePc on Au(111)[52] and CoTPP on Ag(111).[53]

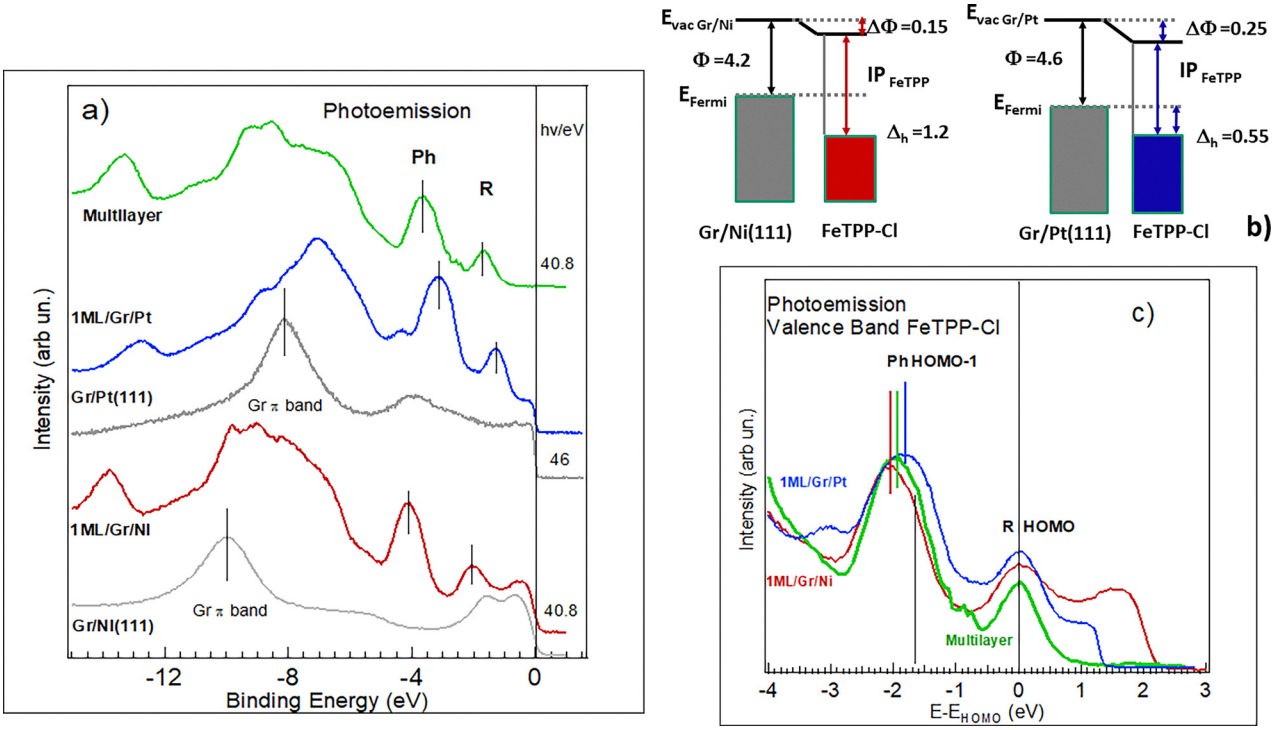

Fig. 2 (a) Valence band spectra of the FeTPP–Cl multilayer (green), 1 ML FeTPP–Cl/Gr/Ni(111) (red), and FeTPP–Cl/Gr/Pt(111) (blue). Graphene spectra on Ni and Pt are shown in grey. π-band positions at 10.0 eV (Ni) and 8.1 eV (Pt) reflect doping differences. The photon energies used for the different spectra are indicated. (b) Schematic representation of the energy level alignment and hole injection barriers for the deposition of FeTPP–Cl on Gr/Ni(111), and Gr/Pt(111) in the monolayer regime. (c) Zoomed-in view of the HOMO–HOMO−1 region showing relative shifts and peak separations; FeTPP–Cl Multilayer (green curve), and 1 ML FeTPP–Cl (red and blue curves), energies are relative to the HOMO peak.

Table 1 Valence band photoemission and secondary cutoff results of the 1 ML deposition of FeTPP–Cl on Gr/Ni(111) and Gr/Pt(111), bare graphene systems and FeTPP–Cl multilayer: HOMO, HOMO onset, HOMO−1, work function (WF), ionization potential (IP)

System	FeTPP–Cl thickness (ML)	HOMO BE (eV)	HOMO onset BE (eV)	HOMO−1 BE (eV)	Work function WF (eV)	IP (eV)
Multilayer	10	1.6	0.9	3.8	4.25	5.1
Gr/Ni(111)	0	—	—	—	4.2	
FeTPP/Gr/Ni	1	2.15	1.2	4.1	4.05	5.25
Gr/Pt(111)	0	—	—	—	4.6	
FeTPP–Cl/Gr/Pt	1	1.2	0.55	3.0	4.35	4.95

Notably, recent studies of FePc adsorption on a Gr/ferromagnetic cobalt surface show that, despite physisorption, the molecule induces an energetically localized hybrid state close to the Fermi level at the K point of Gr.[54] This interface state is interpreted as a charge transfer from Gr to the molecular macrocycle, with the Gr doping slightly changed (about 0.2 eV). This phenomenon has been interpreted as an overlap between the Gr pz state and the molecular macrocycle with partial occupation of the lowest unoccupied molecular orbital (LUMO). In the present work, we do not observe any difference in the N K edge LUMO lineshape of the 1 ML FeTPP–Cl on Ni and the multilayer (Fig. S3 and S4), thus suggesting no contribution of the macrocycle. The interfacial state could be due to the weak hybridization of partially empty out-of-plane d_{z^2} orbitals of Fe with the hybrid d–π states of Ni–Gr.

Our angle-integrated valence band spectra of 1 ML layers (Fig. 2a) do not allow for unambiguous distinction of the graphene π peak, due to the overlap with molecular features (see multilayer VB Fig. S6). In any case, the existence of an interfacial state in the case of Ni is associated with a weak mixing of the substrate with the molecule. Conversely, the absence of the interface state in the Pt case supports our interpretation that significant charge transfer is present on Gr/Ni.

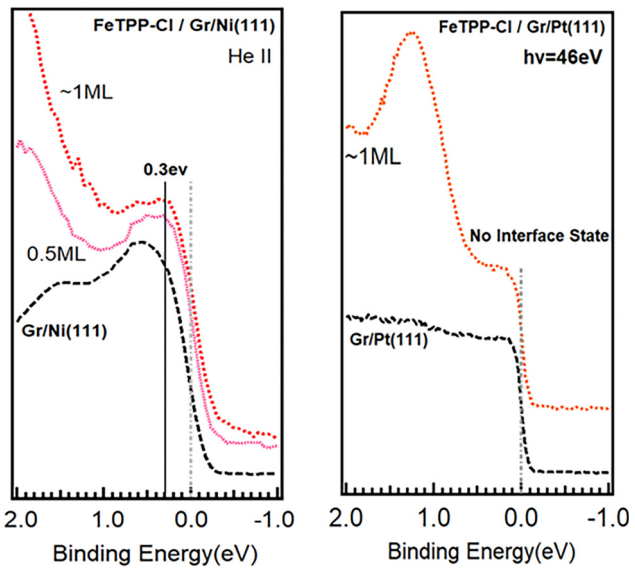

Fig. 3 Valence band spectra close to the Fermi level for the 1 ML FeTPP–Cl on Gr/Ni(111) (left) and Gr/Pt(111) (right). An interface state Is is observed at 0.3 eV for FeTPP–Cl/Gr/Ni(111).

Core level photoemission measurements

To further investigate the molecule–substrate interaction, we characterized the samples by core-level X-ray photoemission spectroscopy (XPS). Fig. 4 compares the N 1s and C 1s spectra of the monolayer systems and the multilayer.

For monolayer coverage, the N 1s peak (Fig. 4a) shifts by 0.2 eV to higher BE with respect to the multilayer in the case of the Gr/Ni substrate, while it moves in the opposite direction by 0.6 eV to lower BE compared with a thick film for the Gr/Pt case. The N 1s spectra are fitted by a single Voigt feature in all three cases. It is worth noting that the single peak excludes the presence of metal-free porphyrin on the surface.[55]

The C 1s spectra (Fig. 4b) are more complex due to multiple C contributions within the FeTPP–Cl molecule (Fig. 4c). At multilayer coverage, the spectrum is deconvoluted into four components (phenyl component A light blue peak, pyrrole C–N–C B red peak, pyrrole C–C peak C yellow peak, C-bridge D green peak, as described in Table S1) with an intensity ratio consistent with the number of equivalent carbon atoms. Carbon C 1s spectra highlight a notable difference between the Ni and Pt substrates. The pristine graphene C 1s peak (gray shadow curves in Fig. 4b) is found at 284.8 eV for Gr/Ni(111) and 283.9 eV for the Gr/Pt, reflecting the different n and p doping, respectively, in agreement with the literature.[56,57] After the molecular deposition, the C 1s spectra become more structured, reflecting a superposition of Gr and molecule-related features. Deconvolution analysis by Voigt curve components identifies four molecular components in agreement with the model used for ZnTPP/Ag(110)[46] and ZnTPP/Si(111).[39]

In the FeTPP–Cl/Gr/Ni(111), carbon phenyl rings of the molecules (a peak in Fig. 4b) overlap with the Gr peak, making it challenging to differentiate between them reliably (see the fit of Fig. S7, and the related discussion). In the FeTPP–Cl/Gr/Pt(111) the Gr is overlaid with the C–C pyrrolic molecular component (labelled C in the fit of Fig. S7). Nonetheless, the pyrrolic C–N–C component (peak B reported in Fig. 4b, by dotted lines) remains distinguishable in both cases, with a BE of 285.3 eV on Ni and 284.7 eV on Pt, compared to 285.2 eV in the multilayer. The shifts in Peak B are correlated with the distinct doping environments: +0.1 eV for Ni (n-doped) and −0.5 eV for Pt (p-doped), *i.e.* in agreement with the trends observed in the valence band and the N 1s spectra. Additionally, the peak B exhibits BE shift relative to the pristine graphene C 1s peak of +0.5 eV and +0.8 eV for Gr/Ni and Gr/Pt, respectively. Detailed fitting components and their BE values are provided in the SI Fig. S6 and Table S1.

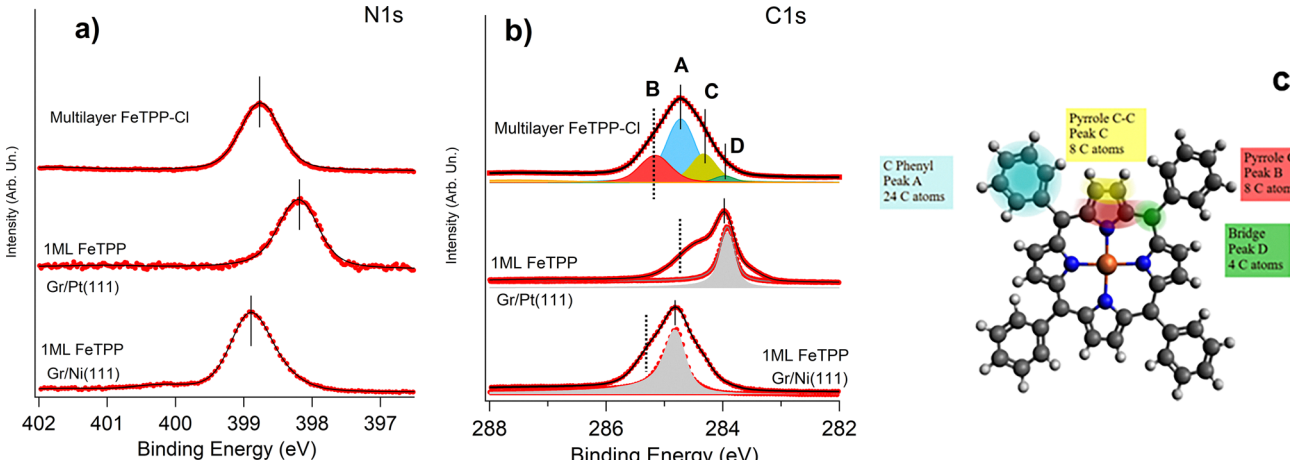

Fig. 4 (a) N 1s and (b) C 1s photoemission spectra taken at *hv* = 525 eV of the multilayer and 1 ML FeTPP–Cl on Gr/Ni(111) and Gr/Pt(111). The feature labeled B in the (b) panel indicates the B (pyrrole C–N–C) component obtained from fitting procedures. Tetraphenylporphyrins consist of four peripheral phenyl rings linked to the central tetrapyrrolic macrocycle (c). See text for details.

Fig. S8 shows the photoemission spectra of the Fe $2p_{3/2}$ core level for both 1 ML and multilayer FeTPP–Cl and FePc coverages. The core level exhibits a complex multiplet structure, characteristic of open-shell elements, which can be described by Zeeman-like final state effects or by the splitting of states according to the total angular momentum. The Fe $2p_{3/2}$ curve-fitting analysis in Fig. S8 is based on the main discernible components, without attempting a full resolution of the multiplet structure.[18,58]

While iron in the multilayer is mainly in the +3 oxidation state,[59] the Fe $2p_{3/2}$ spectra of both monolayers do not clearly exhibit the shake-up features typical of Fe^{3+} at about 715 eV (labelled P′ in the Fig. S8 multilayer), a result similar to the Fe^{2+} of FePc, and suggesting that iron predominantly remains in the Fe(II) state in the two 1 ML samples.[60,61] The Fe $2p_{3/2}$ shows a pronounced shift at higher BE in the case of Gr/Ni(111). A detailed analysis of the 1 ML Fe $2p_{3/2}$ lineshape and a comparison with the spectrum of FePc (Fe^{2+}) (Fig. S8) reveal only slight differences between the two substrates.

Discussion

The spectroscopic results indicate that the interaction of FeTPP–Cl with graphene depends strongly on the underlying metal support. To gain insight into the interfacial charge redistribution mechanisms, we compared the core-level binding energies of FeTPP in monolayer (1 ML) configurations on Gr/Ni(111) and Gr/Pt(111) substrates with those of the multilayer reference. Table 2 summarizes the measured ionization potentials and core-level BEs. Fig. 5 reports the binding energy diagrams of the investigated systems. Core levels and frontier molecular states are compared to multilayer references. The green arrows indicate the direction of the BE shifts: positive, higher BE; negative, lower BE.

The BE of the core levels and the HOMO and HOMO−1 states are indicated and the interface state in FeTPP–Cl/Gr/Ni(111) is labelled Is.

No new spectral components are detected in the 1 ML systems. Combined with the valence band spectra and the small work function (WF) variations, this indicates weak molecule–substrate interactions in both cases.

The measured interface dipoles are −0.15 eV for Gr/Ni(111) and −0.25 eV for Gr/Pt(111). However, WF variation alone is not a direct measure of interaction strength, since it results from competing contributions including the push-back effect (Pauli repulsion), charge transfer, polarization, and charge rearrangement.[62]

The ionization potential, defined as the minimum energy required to remove one electron from a molecule, reflects the intrinsic electronic structure (absolute HOMO energy).[63,64] In the absence of charge transfer, the IP should remain constant

Table 2 Photoemission results for the FeTPP–Cl multilayer and 1 ML films on Gr/Ni(111) and Gr/Pt(111). Reported values include ionization potential (IP) and binding energies (BE) of C 1s in the graphene bare substrate (Gr peak) and C 1s molecular pyrrole (peak B), N 1s, (Fig. 4) and Fe $2p_{3/2}$ main component D in Fig. S8. BE errors: ±0.1 eV for C 1s and Fe $2p_{3/2}$, ±0.05 eV for the others

System	FeTPP–Cl thickness (ML)	IP (eV)	C 1s Gr peak/BE (eV)	C 1s pyrrole C–N–C peak B BE (eV)	N 1s BE (eV)	Fe $2p_{3/2}$ main component D peak BE (eV)
Multilayer	10	5.1		285.2	398.8	707.9
Gr/Ni(111)	0		284.8		—	—
	1	5.25	284.8	285.3	399.0	708.5
Gr/Pt(111)	0		283.9		—	—
	1	4.95	283.9	284.7	398.2	708.0

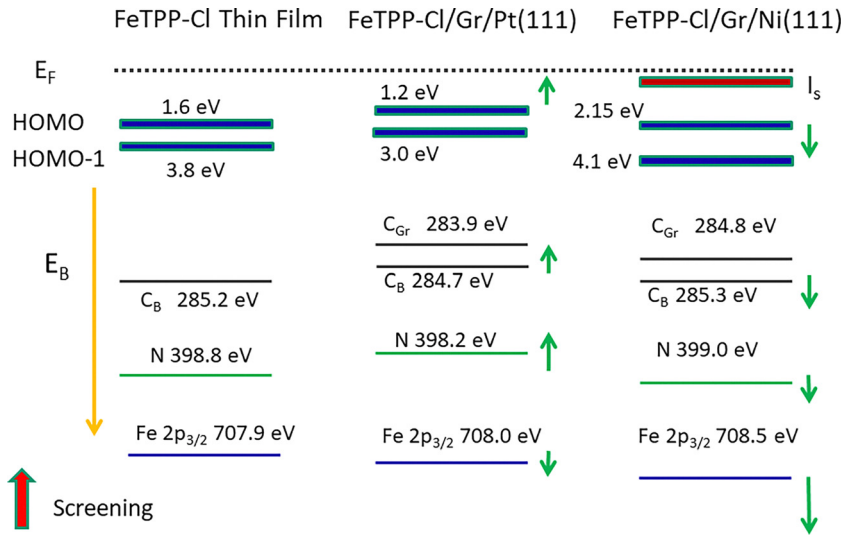

Fig. 5 Binding energy diagrams (not to scale) for the FeTPP–Cl multilayer, FeTPP–Cl/Gr/Ni(111), and FeTPP–Cl/Gr/Pt(111). Core levels and frontier molecular states are compared to multilayer references. Arrows indicate the direction of the shifts: positive (towards higher BE) corresponds to electron transfer from substrate to molecule; negative (towards lower BE) indicates electron donation from molecule to substrate. The screening effect is discussed in paragraph S7 and ref. 71.

across substrates. This has been demonstrated, for example, in electron-rich triphenylene derivatives adsorbed on both Gr/Ni(111) and metallic substrates.[65] By contrast, when charge transfer occurs, its magnitude and direction depend on the substrate.[66]

In our case, the IP increases on FeTPP–Cl n-doped graphene (Gr/Ni) and decreases on p-doped graphene (Gr/Pt) compared to the multilayer. These opposite shifts suggest different charge transfer directions. Since the only difference between the two systems is the underlying metal (which determines the graphene doping), the results strongly support substrate-dependent charge transfer, with opposite directions on Ni and Pt.

This finding is consistent with theoretical calculations showing opposite HOMO shifts for FeTPP adsorbed on Au(111) *versus* Cu(111)/Ag(111).[48] Adsorption on Au(111) shifts the occupied states closer to the Fermi level, facilitating charge transfer from the molecule to the substrate (similar to our Gr/Pt case). Conversely, adsorption on Ag(111) or Cu(111) shifts the HOMO to higher BE and the unoccupied states downward, favoring charge transfer from the substrate to the molecule (similar to our Gr/Ni case). The HOMO positive shift at higher BE is interpreted as an injection of electrons to the molecule, even in studies based on potassium doping of molecular layers.[67]

Overall, the small interface dipoles (−0.15 eV on Ni, −0.25 eV on Pt) and modest IP changes (below ±0.25 eV) confirm weak physisorption mediated by graphene, with electronic modulation governed primarily by electrostatic and polarization screening effects rather than strong hybridization.[63,68] This is consistent with established principles of Fermi-level alignment. It is worth noting that the IP difference and positive HOMO shift in the case of FeTPP–Cl/Gr/Ni suggest a charge transfer that should lead to an increase in the work function as found in the case of FePc/Gr/Ni(111).[32,33]

For FeTPP–Cl/Gr/Ni(111), we observe positive BE shifts of all core levels compared to the multilayer, most notably a +0.6 eV shift in Fe 2p. The large Fe 2p shift, much stronger than in C 1s or N 1s, indicates a pronounced involvement of the Fe center in charge redistribution. Together with the IP increase (+0.15 eV), this supports net electron transfer from the substrate to the molecule. We therefore propose that the interface state (Is in Fig. 5) is at least partially localized at the Fe center.

In contrast, FeTPP–Cl/Gr/Pt(111) shows negative shifts for C 1s and N 1s, consistent with electron depletion of the porphyrin macrocycle. The IP decrease (−0.15 eV) indicates electron transfer from the molecule to the substrate. The small Fe 2p shift (+0.1 eV, within error) suggests that the charge redistribution is more delocalized on the macrocycle rather than the Fe ion. Thus, the two systems exhibit opposite charge transfer directions: electron acceptance in the Gr/Ni(111) case and electron donation in the Gr/Pt(111) case.

The absence of rigid shifts in the core-level spectra of 1 ML in relation to the multilayer, further highlights that charge redistribution occurs non-uniformly within the molecule. Different parts of FeTPP–Cl are influenced to different extents by the substrate doping and local electrostatic environment, consistent with prior reports of fractional charge transfer at molecule–substrate interfaces.[69] Such non-rigid shifts contrast with the rigid core-level shifts typical of homogeneous physisorption, and instead indicate internal electronic rearrangements within the molecule. Non-isotropic charge transfer has been demonstrated for FePc/Cu(111)[70] through STM, core-level photoemission, and theoretical calculations, highlighting specific contributions from different molecular groups.

A reduced charge transfer for FeTPP–Cl/Gr/Pt(111) can be rationalized by the larger graphene–metal separation (0.30 nm for Pt *vs.* 0.25 nm for Ni), which weakens substrate–adsorbate coupling. This agrees with the absence of an interface state in the valence band of the Pt system.

Finally, our observations align partially with recent theoretical studies of FeTPP on freestanding graphene. Song *et al.*[35] reported negligible charge transfer and orbital perturbation, consistent with weak physisorption. In contrast, Touzeau *et al.*[36] found that subtle structural or geometric changes can induce detectable charge redistribution. Our finding of opposite charge transfer directions on Ni and Pt substrates—despite identical adsorbates and single-layer morphology—supports the latter view and highlights the critical role of the underlying metal in modulating charge transfer across graphene. Future theoretical work is needed to fully enlighten these effects.

Conclusions

Our work aims to exploit the potential of graphene to tune interfacial electronic properties and gain control over charge transfer processes, injection barriers, and charge transport, key parameters in the design of next-generation organic electronic devices. By comparing n-doped graphene on Ni and p-doped graphene on Pt, we demonstrate that substrate selection is a powerful strategy to modulate the electronic behavior of hybrid porphyrin-based nanostructures. Our data show that introducing a graphene buffer layer at the organic–metal interface allows for significant tuning of molecule–surface interactions. Specifically, we investigated how the electronic structure of FeTPP–Cl monolayers is influenced by the underlying substrate *via* the graphene interlayer. Despite the similar molecular morphology of FeTPP–Cl on both Gr/Ni(111) and Gr/Pt(111), significant differences emerge in interfacial charge redistribution and level alignment.

The non-rigid shifts observed in N 1s, the various C 1s components, and Fe 2p core levels imply that the electrostatic environment created by the underlying substrate (through doping and screening) affects various parts of the molecule differently. This leads to an internal redistribution of electronic density within the FeTPP–Cl molecule rather than a uniform, rigid shift of all energy levels, consistent with prior studies on molecule–substrate interactions through graphene.

The Ni substrate induces electron transfer to the molecule, strongly involving the Fe center, whereas the Pt substrate drives electron donation from the molecule, centered on the C and N framework. These opposite charge transfer directions arise from the doping and electronic screening imposed by the underlying metal, rather than direct chemical bonding. The absence of rigid spectral shifts further points to fractional, non-uniform redistribution within the molecule. Taken together, these results show that graphene serves as an effective mediator, allowing subtle substrate-dependent tuning of molecular electronic states. Such control over interfacial charge transfer is essential for engineering molecule–graphene–metal heterostructures in electronic and catalytic applications.

This work demonstrates the pivotal role of the graphene buffer layer and its underlying metal substrate in tailoring the electronic structure of hybrid graphene–porphyrin systems. Although the overlapping of molecular and graphene features complicates a precise assessment of doping changes upon adsorption, the core-level analysis reveals a distinct rearrangement of electronic charge in the two systems. Understanding and controlling this bidirectional charge transfer is crucial for engineering functional molecular interfaces.

Overall, our results point to two main strategies for tuning the adsorption and electronic behavior of tetrapyrrole complexes on graphene: (1) modifying the metal center in the molecule to influence supramolecular organization at sub-monolayer coverages, and (2) selecting the appropriate substrate beneath graphene to control molecule–graphene coupling *via* charge transfer. These insights advance our understanding of molecule–graphene–metal interfaces and guide strategies for tuning electronic properties in hybrid systems through controlled substrate engineering.

Author contributions

C. C., M. P. and A. G. conceived and planned the work and the experiments, contributed to the growth of the samples and carried out the measurements. A. N., E. M., F. B., I. P., A. K. S. N., M. P. M. S., and L. C. performed the measurements. M. S. and A. K. performed the data analysis and wrote the preliminary draft manuscript; both contributed equally to this work. M. S., C. C and M. P., I. P. refined the data analysis and wrote the final version of the paper. The manuscript was written through the contributions of all authors. All authors have approved the final version of the manuscript.

Conflicts of interest

There are no conflicts to declare.

Data availability

We have provided the data in the main manuscript and in the supplementary information (SI). Supplementary information is available. See DOI: **https://doi.org/10.1039/d5tc01982f**.

Any further data is available from the corresponding author upon reasonable request.

Acknowledgements

The authors want to thank HZB for the allocation of synchrotron radiation beamtime at BESSY II (HESGM beamline) *via* projects 14100661 and 14201002 and ELETTRA (Sincrotrone Trieste) *via* proposals 20180321 and 20175485 at the BACH Beamline. The European Union has funded this work by NextGenerationEU, Mission 4, Component 2, under the Italian Ministry of University and Research (MUR) National Innovation Ecosystem grant ECS00000041 - VITALITY - CUP B43C22000470005. The CNR-IOM technical staff members, Stefano Bigaran, Federico Salvador, Stefano Cristiani, Davide Benedetti, and Andrea Martin, are kindly acknowledged for their support.

References

1 M. Fahlman, S. Fabiano, V. Gueskine, D. Simon, M. Berggren and X. Crispin, *Nat. Rev. Mater.*, 2019, **4**, 627.
2 J. Yang, D. Yan and T. S. Jones, *Chem. Rev.*, 2015, **115**, 5570.
3 B. Song, C. Rolin, J. D. Zimmerman and S. R. Forrest, *Adv. Mater.*, 2014, **26**, 2914.
4 C. Wang, H. Dong, W. Hu, Y. Liu and D. Zhu, *Chem. Rev.*, 2012, **112**, 2208.
5 D. G. Papageorgiou, I. A. Kinloch and R. J. Young, *Prog. Mater. Sci.*, 2017, **90**, 75.
6 C. Lee, X. Wei, J. W. Kysar and J. Hone, *Science*, 2008, **321**, 385.
7 S. V. Morozov, K. S. Novoselov, M. I. Katsnelson, F. Schedin, D. C. Elias, J. A. Jaszczak and A. K. Geim, *Phys. Rev. Lett.*, 2008, **100**, 016602.
8 A. A. Balandin, S. Ghosh, W. Bao, I. Calizo, D. Teweldebrhan, F. Miao and C. N. Lau, *Nano Lett.*, 2008, **8**, 902.
9 V. B. Mohan, K. Jayaraman and D. Bhattacharyya, *Solid State Commun.*, 2020, **320**, 114004.
10 M. Batzill, *Surf. Sci. Rep.*, 2012, **67**, 83.
11 E. N. Voloshina and Y. S. Dedkov, *Phys. Chem. Chem. Phys.*, 2014, **14**, 13502.
12 E. N. Voloshina and Y. S. Dedkov, *Mater. Res. Express*, 2014, **1**, 035603.
13 H. Lee, K. Paeng and I. S. Kim, *Synth. Met.*, 2018, **244**, 36.
14 L. L. Patera, C. Africh, R. S. Weatherup, R. Blume, S. Bhardwaj, C. Castellarin-Cudia, A. Knop-Gericke, R. Schloegl, G. Comelli, S. Hofmann and C. Cepek, *ACS Nano*, 2013, **7**, 7901.
15 G. Giovannetti, P. A. Khomyakov, G. Brocks, V. M. Karpan, J. van den Brink and P. J. Kelly, Doping graphene with metal contacts, *Phys. Rev. Lett.*, 2008, **101**, 026803.
16 P. Sutter, J. T. Sadowski and E. Sutter, Graphene on Pt(111), *Phys. Rev. B: Condens. Matter Mater. Phys.*, 2009, **80**, 245411.
17 M. Gao, Y. Pan, L. Huang, H. Hu, L. Z. Zhang, H. M. Guo, S. X. Du and H.-J. Gao, *Appl. Phys. Lett.*, 2011, **98**, 03310.
18 J. M. Gottfried, *Surf. Sci. Rep.*, 2015, **70**, 259.
19 C.-A. Palma and P. Samorì., *Nat. Chem.*, 2011, **3**, 431.
20 C. Waeckerlin, K. Tarafder, D. Siewert, J. Girovsky, T. Haehlen, C. Iacovita, A. Kleibert, F. Nolting, T. A. Jung, P. M. Oppeneer and N. Ballav, *Chem. Sci.*, 2012, **3**, 3154.
21 Z. Dai, Q. Sun, X. Liu, C. Bian, Q. Wu, S. Pan, L. Wang, X. Meng, F. Deng and F.-S. Xiao, *J. Catal.*, 2016, **338**, 202.
22 W. Hao, D. Chen, Y. Li, Z. Yang, G. Xing, J. Li and L. Chen, *Chem. Mater.*, 2019, **31**, 8100.
23 J. S. O'Neill, L. Kearney, M. P. Brandon and M. T. Pryce, *Coord. Chem. Rev.*, 2022, **467**, 214599.
24 Z. Liang, H. Y. Wang, H. Zheng, W. Zhang and R. Cao, *Chem. Soc. Rev.*, 2021, **50**, 2540.
25 R. Paolesse, S. Nardis, D. Monti, M. Stefanelli and C. Di Natale, *Chem. Rev.*, 2017, **117**, 2517–2583.
26 O. G. Ziogos, I. Blanco and J. Blumberger, *J. Chem. Phys.*, 2020, **153**, 44702.
27 M. Abdinejad, A. Farzi, R. Möller-Gulland, F. Mulder, C. Liu, J. Shao, J. Biemolt, M. Robert, A. Seifitokaldani and T. Burdyny, *Nat. Catal.*, 2024, **7**, 1109–1119.
28 M. L. Pegis, D. J. Martin, C. F. Wise, A. C. Brezny, S. I. Johnson, L. E. Johnson, N. Kumar, S. Raugei and J. M. Mayer, *J. Am. Chem. Soc.*, 2019, **141**, 8315–8326.
29 F. Armillotta, D. Bidoggia, P. Biasin, A. Annese, A. Cossaro, A. Verdini, M. Peressi and E. Vesselli, *Cell Rep. Phys. Sci.*, 2023, **4**, 101378.
30 V. D. Pham, J. Lagoute, O. Mouhoub, F. Joucken, V. Repain, C. Chacon, A. Bellec, Y. Girard and S. Rousset, *ACS Nano*, 2014, **8**, 9403.
31 J. Uihlein, M. Polek, M. Glaser, H. Adler, R. Ovsyannikov, M. Bauer, M. Ivanovic, A. B. Preobrajenski, A. V. Generalov, T. Chassé and H. Peisert, *J. Phys. Chem. C*, 2015, **119**, 15240.
32 J. Uihlein, H. Peisert, H. Adler, M. Glaser, M. Polek, R. Ovsyannikov and T. Chassé, *J. Phys. Chem. C*, 2014, **118**, 10106–10112.
33 Y. Wei-Guo, L. Dan, P. Xiao-Feng and D. Wei-Dong, *Chin. Phys. B*, 2013, **22**, 117301.
34 P. Li and Z.-H. Lu, *Small Sci.*, 2021, **1**, 2000015.
35 Y.-J. Song, C. Gallenkamp, G. Lleopart, V. Krewald and R. Valentı, *Phys. Chem. Chem. Phys.*, 2024, **26**, 26370–26376.
36 J. Touzeau, F. Barbault, F. Maurel and M. Seydou, *Chem. Phys. Lett.*, 2018, **713**, 172–179.
37 J. Stoehr, *NEXAFS Spectroscopy*, Berlin Verlag, 1992.
38 W. Auwärter, K. Seufert, F. Klappenberger, J. Reichert, A. Weber-Bargioni, A. Verdini, D. Cvetko, M. Dell'Angela, L. Floreano, A. Cossaro, G. Bavdek, A. Morgante, A. P. Seitsonen and J. V. Barth, *Phys. Rev. B: Condens. Matter Mater. Phys.*, 2010, **81**, 245403.
39 C. Castellarin-Cudia, P. Borghetti, G. Di Santo, M. Fanetti, R. Larciprete, C. Cepek, P. Vilmercati, L. Sangaletti, A. Verdini, A. Cossaro, L. Floreano, A. Morgante and A. Goldoni, *Chem. Phys. Chem.*, 2010, **11**, 2248.
40 V. A. Karachevtseva, S. G. Stepanian, M. V. Karachevtsev and L. Adamowicz, *Comput. Theor. Chem.*, 2018, **1**, 1133.
41 M. Bouatou, R. Harsh, F. Joucken, C. Chacon, V. Repain, A. Bellec, Y. Girard, S. Rousset, R. Sporken, F. Gao, M. Brandbyge, Y. J. Dappe, C. Barreteau, A. Smogunov and J. Lagoute, *J. Phys. Chem. Lett.*, 2020, **11**, 9329–9335.
42 **https://www.iom.cnr.it/research-facilities/facilities-labs/analytical-microscopy-and-spectroscopy/inspect/.**
43 M. Zangrando, M. Zacchigna, M. Finazzi, D. Cocco, R. Rochow and F. Parmigiani, *Rev. Sci. Instrum.*, 2004, **75**, 31.
44 A. Calloni, M. S. Jagadeesh, G. Bussetti, G. Fratesi, S. Achilli, A. Picone, A. Lodesani, A. Brambilla, C. Goletti, F. Ciccacci, L. Duò, M. Finazzi, A. Goldoni, A. Verdini and L. Floreano, *Appl. Surf. Sci.*, 2020, **505**, 144213.
45 P. Borghetti, *Self-assembly and electronic properties of macromolecular systems: ordered ultrathin porphyrin layers vs hierarchically assembled eumelanin thin films*, PhD Thesis, Università Cattolica del sacro cuore, Brescia A. A., 2009/2010, site **https://centridiricerca.unicatt.it/ilamp-PhDThesis_BorghettiP.pdf.**
46 G. Di Santo, C. Castellarin-Cudia, M. Fanetti, B. Taleatu, P. Borghetti, L. Sangaletti, L. Floreano, E. Magnano, F. Bondino and A. Goldoni, *J. Phys. Chem. C*, 2011, **115**, 4155.

47 M. Nardi, R. Verucchi, C. Corradi, M. Pola, M. Casarin, A. Vittadini and S. Iannotta, *Phys. Chem. Chem. Phys.*, 2010, **12**, 871.
48 H. Tang, N. Tarrat, V. Langlais and Y. Wang, *Beilstein J. Nanotechnol.*, 2017, **8**, 2484. 49.
49 X. Li, A. Feng, Y. Zu, P. Liu and F. Han, *Molecules*, 2023, **28**, 3452.
50 D. Nobis, M. Potenz, D. Niesner and T. Fauster, *Phys. Rev. B: Condens. Matter Mater. Phys.*, 2013, **88**, 195435.
51 L. Massimi, S. Lisi, D. Pacilè, C. Mariani and M. G. Betti, *Beilstein J. Nanotechnol.*, 2014, **5**, 308.
52 S. Ahmadi, M. N. Shariati, S. Yu and M. Göthelid, *J. Chem. Phys.*, 2012, **137**, 084705.
53 T. Lukasczyk, K. Flechtner, L. R. Merte, N. Jux, F. Maie, J. M. Gottfried and H.-P. Steinrück, *J. Phys. Chem. C*, 2007, **111**, 3090.
54 I. Cojocariu, D. Perilli, V. Feyer and M. Jugovac, *Chem. – Eur. J.*, 2024, **30**, e202400857.
55 M. Panighel, *Adsoprtion, Metalation and Magnetic Properties of Tetraphenyl Porphrins on Metal Surfaces*, PhD Thesis, Università Trieste a.a., 2013–2014.
56 P. K. Nayak, C. J. Hsu, S. C. Wang, J. C. Sung and J. L. Huang, *Thin Solid Films*, 2013, **529**, 312.
57 C. Oshima and A. Nagashima, *J. Phys.: Condens. Matter*, 1997, **9**, 1.
58 M. Schmid, J. Zirzlmeier, H. P. Steinrück and J. M. Gottfried, *J. Phys. Chem. C*, 2011, **115**, 17028.
59 A. M. El-Mahalawy, A. M. Nawar and A. R. Wassel, *J. Mater. Sci.*, 2022, **57**, 15413–15439.
60 A. P. Grosvenor, B. A. Kobe, M. C. Biesinger and N. S. McIntyre, *Surf. Interface Anal.*, 2004, **36**, 1564–1574.
61 M. Biesenger, *et al.*, *Appl. Surf. Sci.*, 2011, **257**, 2717–2730.
62 N. Koch, A. Kahn, J. Ghijsen, J.-J. Pireaux, J. Schwartz, R. L. Johnson and A. Elschner, *Appl. Phys. Lett.*, 2003, **82**, 70–72.
63 I. G. Hill, A. Rajagopal, A. Kahn and Y. Hu, *Appl. Phys. Lett.*, 1998, **73**, 662.
64 S. Duhm, G. Heimel, I. Salzmann, H. Glowatzi, R. L. Johnson, A. Vollmer, J. P. Rabe and N. Koch, *Nat. Mater.*, 2008, **7**, 326–332.
65 J. de la Rie, Q. Wang, M. Enache, M. Kivala and M. Stöhr, *J. Phys. Chem. C*, 2024, **128**, 11014–11023.
66 S. Park, T. Schultz, D. Shin, N. Mutz, A. Aljarb, H. S. Kang, C.-H. Lee, L.-J. Li, X. Xu, V. Tung, E. J. W. List-Kratochvil, S. Blumstengel, P. Amsalem and N. Koch, *ACS Nano*, 2021, **15**, 14794–14803.
67 C. Cepek, M. Sancrotti, T. Greber and J. Osterwalder, *Surf. Sci.*, 2000, **454–456**, 467–471.
68 H. Ishii and K. Seki, *IEEE Trans. Electron Devices*, 1997, **44**, 1295.
69 S.-A. Savu, G. Biddau, L. Pardini, R. Bula, H. F. Bettinger, C. Draxl, T. Chassé and M. B. Casu, *J. Phys. Chem. C*, 2015, **119**, 12538–12544.
70 O. Snezhkova, J. Lueder, A. Wiengarten, S. R. Burema, F. Bischoff, Y. He, J. Rusz, J. Knudsen, M.-L. Bocquet, K. Seufert, J. V. Barth, W. Auwaerter, B. Brena and J. Schnadt, *Phys. Rev. B: Condens. Matter Mater. Phys.*, 2015, **92**, 075428.
71 T. Aihara, S. A. Abd-Rahman and H. Yoshida, *Phys. Rev. B*, 2021, **104**, 085305.